

# On-line identification of contact dynamics in the presence of geometric uncertainties

Diederik Verscheure\*, Jan Swevers\*, Herman Bruyninckx\*, Joris De Schutter\*

**Abstract**—Robots are increasingly used to perform complex tasks, which often involve interaction and contact with unstructured environments. By identifying geometric uncertainties and the dynamic behavior of the environment on-line, the autonomy of intelligent robot systems can be considerably improved. This paper considers the 2D case of an industrial robot equipped with a probe to explore an unknown environment. The goal is to estimate from the measured end-effector position, velocity and forces not only the environmental contact dynamics parameters, but also geometric parameters such as the environment position and orientation, and the position of the probe end-point with respect to the robot end-effector. To this end, a Kalman filter based algorithm is proposed, which enforces physical constraints and which is executed in an event-triggered way to improve convergence and robustness. Experimental results illustrate the viability of the proposed algorithm.

## I. INTRODUCTION

THE AUTONOMY of intelligent robot systems can be considerably improved by taking into account geometric uncertainties and the dynamic behavior of the environment. Specifically, knowledge of the contact dynamics can be used to increase the robustness of the low-level controllers, while identification of uncertain geometric parameters can be used to improve task execution. Extending the identification skills of robots is essential for applications such as industrial processes, robot surgery and space manipulation.

Initial efforts in on-line identification of contact dynamics were motivated by the problem of identifying the environment stiffness in the context of impedance control [1]–[4], while more recent efforts are also motivated by the need to improve the autonomy of robots [5]–[8]. The dynamics of the environment are typically approximated by a linear spring, spring-damper, or mass-spring-damper model, while the contact dynamics parameters are estimated using adaptive control methods [2], [4], [9], (extended) Kalman filtering [1], [5], recursive least squares [3], [6]–[8].

Most of these methods, however, consider the geometry of the environment to be known or partially known and focus only on identification of the contact dynamics. In contrast, this paper considers both the environment *stiffness and friction* and tackles the contact dynamics identification problem in the presence of *full geometric uncertainties*. Specifically, the case of a typical industrial robot equipped with a probe to explore an unknown environment is considered. The position and velocity of the robot end-effector and the forces acting on the end-effector are measured and the goal is to estimate

not only the environmental contact dynamics parameters, but also geometric parameters such as the environment position and orientation, and the position of the probe end-point with respect to the robot end-effector. The considered case is useful in the context of autonomous environment exploration, and it is also *the archetype* for a lot of tasks involving a robot holding or manipulating in *an* uncertain way *an* unknown object in contact with *an* unknown environment. This paper focuses on a 2D case, although the methodology can be generalized to 3D cases without drastic modifications.

The outline of this paper is as follows. Section II describes the geometric and dynamic modeling approach. Section III defines the nonlinear state space model and proposes a Kalman filter based identification algorithm. Section IV discusses a number of considerations concerning the excitation signals for the identification. Subsequently, the identification algorithm is verified experimentally in Section V. Finally, Section VI discusses conclusions and future work.

## II. MODELING

Section II-A discusses the modeling assumptions, while Section II-B discusses the choice of the contact dynamics models. In Section II-C, the parameter set is chosen and the contact dynamics equations are given.

### A. Modeling assumptions

First, the compliance of the environment is modelled only in the normal direction, such that forces tangential to the environment are assumed to be entirely due to friction. Furthermore, the environment geometry is assumed to be only lightly-curved and the probe mounted on the robot is assumed to be a rigid, sharp object ending in a single vertex. Furthermore, the robot motions are assumed to be sufficiently slow, such that inertial forces may be neglected, while gravity forces are compensated for in the force measurements.

### B. Contact dynamics models

Since this paper considers excitation signals that can be executed by a typical industrial robot, it is unlikely that identification of damping or mass parameters in the force-deformation relation is possible, as this requires excitation signals with frequency contents above a few Hz [8], [9]. Therefore, the force-deformation relation is described by a simple linear spring model

$$F_n(\delta) = \begin{cases} \kappa\delta, & \text{if } \delta > 0, \\ 0, & \text{if } \delta \leq 0, \end{cases} \quad (1)$$

where  $\delta$  and  $\kappa$  are the environment deformation and stiffness.

\* D. Verscheure (e-mail: [diederik.verscheure@mech.kuleuven.be](mailto:diederik.verscheure@mech.kuleuven.be)), J. Swevers, H. Bruyninckx, J. De Schutter are with the Dept. of Mech. Eng., K.U.Leuven, Celestijnenlaan 300B, 3001 Heverlee, Belgium.

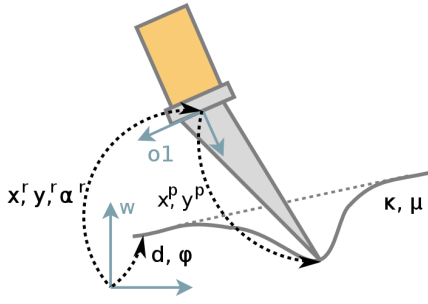


Fig. 1. The geometric parameters and variables.

For the friction model, a Coulomb model variant is chosen

$$F_f(v_t) = \begin{cases} \text{undefined,} & \text{if } |v_t| < v_{t,m} \\ -\text{sgn}(v_t)(\mu F_n), & \text{if } |v_t| \geq v_{t,m}, \end{cases} \quad (2)$$

where  $v_t$  is the relative tangential velocity in the contact,  $\text{sgn}(\cdot)$  is defined as the signum function,  $\mu$  is the coefficient of friction,  $v_{t,m}$  is a threshold velocity. The sticking phase is explicitly chosen *not* to be modelled, and the only requirement for the choice of the threshold velocity  $v_{t,m}$  is that it needs to be large enough, such that model (2) is only used in the sliding phase.

### C. Geometric and dynamic modeling

The choice of the contact dynamics parameters follows logically from the chosen models. In contrast, the choice of the geometric parameters is not unique and does not necessarily result in a minimal description. For the identification, however, it is useful to use a *minimal parameterisation* and to choose geometric variables that are static in the frames in which they are defined, in other words geometric parameters, as this avoids the need for nonlinear constraints between the parameters and nonlinear process equations respectively.

Skipping the details concerning the choice of the parameter set, the parameters describing the geometric uncertainties are  $x^p$  and  $y^p$ , representing the coordinates of the probe end-point in the end-effector frame  $o1$  (Fig. 1), and  $\phi$  and  $d$ , representing the orientation and offset of the environment surface with respect to the world frame  $w$  (Fig. 1). The geometric variables describing the position of the robot with respect to the world frame  $w$  are  $x^r$ ,  $y^r$  and  $\alpha^r$  (Fig. 1).

Once the parameter set has been fixed, the contact dynamics equations can be derived. Omitting the derivation, the relation in the sliding phase, between the measured forces  $F_x$ ,  $F_y$  and  $M_z$ , the measured end-effector position, the geometric and dynamic parameters, and the deformation  $\delta$  and the velocity  $v_t^p$  of the probe end-point tangential to the environment surface, can be written as

$$F_x = \kappa \delta (-\text{sgn}(v_t^p) \mu C_{(\alpha^r - \phi)} + S_{(\alpha^r - \phi)}), \quad (3)$$

$$F_y = \kappa \delta (\text{sgn}(v_t^p) \mu S_{(\alpha^r - \phi)} + C_{(\alpha^r - \phi)}), \quad (4)$$

$$M_z = \kappa \delta (\text{sgn}(v_t^p) \mu (C_{(\alpha^r - \phi)} y^p + S_{(\alpha^r - \phi)} x^p) + (C_{(\alpha^r - \phi)} x^p - S_{(\alpha^r - \phi)} y^p)), \quad (5)$$

where  $C_{(\cdot)}$  and  $S_{(\cdot)}$  are shorthand notations for  $\cos(\cdot)$  and  $\sin(\cdot)$  respectively. The environment deformation  $\delta$  and the tangential velocity of the contact point  $v_t^p$  can also be

rewritten in terms of the measured end-effector position and velocity and the geometric parameters, namely

$$\delta = S_\phi x^r - C_\phi y^r - S_{(\alpha^r - \phi)} x^p - C_{(\alpha^r - \phi)} y^p + d, \quad (6)$$

$$v_t^p = C_\phi \dot{x}^r + S_\phi \dot{y}^r - (S_{(\alpha^r - \phi)} x^p + C_{(\alpha^r - \phi)} y^p) \dot{\alpha}^r. \quad (7)$$

Using equations (6) and (7),  $\delta$  and  $v_t^p$  can be eliminated so that the equations (3)-(5) depend only on the force measurements, the robot end-effector position and velocity measurements, and the geometric and dynamic parameters.

## III. IDENTIFICATION

In this section, a state space representation for the chosen geometric and dynamic parameters and the states of the system is constructed. The states are the dynamic variables which describe the state of the combined system of the robot and the environment, namely the position and velocity of the robot. The *process equation* is specified in Section III-A, and the *measurement equation* is defined in Section III-B. Section III-C proposes a Kalman filter based algorithm, which is executed in an event-triggered way as explained in Section III-D to improve convergence and robustness.

### A. Process equation for the parameters and states

Since the measured end-effector position and velocity may be noisy and the end-effector acceleration is bounded and usually exhibits some form of continuity, the accuracy of the estimated position and velocity can be improved by including the end-effector acceleration as a state variable and tracking these quantities with a white-noise jerk process model [10]

$$\begin{pmatrix} \mathbf{x}_k^p \\ \mathbf{x}_k^v \\ \mathbf{x}_k^a \end{pmatrix} = \begin{pmatrix} 1 & T_s & \frac{T_s^2}{2} \\ 0 & 1 & T_s \\ 0 & 0 & 1 \end{pmatrix} \begin{pmatrix} \mathbf{x}_{k-1}^p \\ \mathbf{x}_{k-1}^v \\ \mathbf{x}_{k-1}^a \end{pmatrix} + \begin{pmatrix} \epsilon_{k-1}^p \\ \epsilon_{k-1}^v \\ \epsilon_{k-1}^a \end{pmatrix}, \quad (8)$$

where  $T_s$  is the sample time,  $\epsilon_{k-1}^p$ ,  $\epsilon_{k-1}^v$  and  $\epsilon_{k-1}^a$  are Gaussian noise vectors and where  $\mathbf{x}_k^p = (x_k^r, y_k^r, \alpha_k^r)^T$ ,  $\mathbf{x}_k^v = (\dot{x}_k^r, \dot{y}_k^r, \dot{\alpha}_k^r)^T$  and  $\mathbf{x}_k^a = (\ddot{x}_k^r, \ddot{y}_k^r, \ddot{\alpha}_k^r)$  represent the end-effector position, velocity and acceleration.

For the geometric and dynamic parameters, which may be slowly varying, very often, the process equation is chosen as

$$\mathbf{x}_k^s = \mathbf{x}_{k-1}^s + \epsilon_{k-1}^s, \quad (9)$$

where  $\epsilon_{k-1}^s$  is a Gaussian noise vector and  $\mathbf{x}_k^s$  contains the geometric and dynamic parameters at time-step  $k$ , namely  $\mathbf{x}_k^s = (x_k^p, y_k^p, \phi_k, d_k, \kappa_k, \mu_k)^T$ . However, process equation (9) implicitly assumes that the parameters *vary with time*, while it is *more reasonable* to assume that they vary with the position of the contact point on the environment surface. Furthermore, process equation (9) is unreasonable for *physically constrained parameters*, such as the environment stiffness which is *always positive*, since the model expresses that the stiffness *can become negative* at any time.

To solve the first problem, the uncertainty on the geometric and dynamic parameters is increased only when the contact point has moved by a certain threshold amount. The second problem can be solved by a reparameterisation. Instead of assuming  $\kappa_k$  and  $\mu_k$  to have a Gaussian distribution for a given  $\kappa_{k-1}$  and  $\mu_{k-1}$ , as expressed by model (9), they can

be assumed to have a Johnson distribution [11]. Specifically, if a variable  $x$  is known to have an upper bound  $x_u$  and lower bound  $x_l$  and only the mean and standard deviation are known, then the least informative distribution which summarizes this information is the Johnson distribution

$$p(x) = \frac{\exp\left(-\ln\left(\frac{x-x_l}{x_u-x}\right) - \gamma\right)/(2\sigma^2)}{\sqrt{2\pi}\sigma(x-x_l)(x_u-x)} = \mathcal{J}(x; \gamma, \sigma; x_l, x_u),$$

for  $x \in [x_l, x_u]$ .  $\gamma$  and  $\sigma$  are *not* actually the mean and standard deviation of  $x$ , although they determine the mean and standard deviation. Furthermore, if  $x \sim \mathcal{J}(x; \gamma, \sigma; x_l, x_u)$  then  $s = \ln\left(\frac{x-x_l}{x_u-x}\right)$  has a Gaussian distribution

$$p(s) = \frac{1}{\sqrt{2\pi}\sigma} \exp\left(-\frac{(s-\gamma)^2}{2\sigma^2}\right) = \mathcal{N}(s; \gamma, \sigma), \quad (10)$$

where  $s \in \mathcal{R}$  and  $x = (\exp(s)x_u + x_l)/(\exp(s) + 1)$ . Using this knowledge, instead of estimating  $\kappa_k$  and  $\mu_k$  directly,

$$\tilde{\kappa}_k = \ln\left(\frac{\kappa_k - 0}{\bar{\kappa} - \kappa_k}\right) \quad \text{and} \quad \tilde{\mu}_k = \ln\left(\frac{\mu_k - 0}{\bar{\mu} - \mu_k}\right) \quad (11)$$

are estimated instead, such that  $\kappa_k$  and  $\mu_k$  are restricted to lie in  $[0, \bar{\kappa}]$  and  $[0, \bar{\mu}]$  respectively. Because of the reparameterisation, the parameter vector is changed to

$$\mathbf{x}_k^s = (x_k^p, y_k^p, \phi_k, d_k, \tilde{\kappa}_k, \tilde{\mu}_k)^T \quad (12)$$

and process equation (9) is adopted for the modified parameter vector. Equation (9) correctly specifies that  $\tilde{\kappa}_k$  and  $\tilde{\mu}_k$  can evolve in an unconstrained way, implying that  $\kappa_k$  and  $\mu_k$  evolve in a constrained way.

### B. Measurement equation

The measurement equation relates the measurements to the geometric and dynamic parameters and the states as

$$\begin{pmatrix} \mathbf{z}_{w,k} \\ \mathbf{z}_{p,k} \\ \mathbf{z}_{v,k} \end{pmatrix} = \begin{pmatrix} \mathbf{h}_w(\mathbf{x}_k^s, \mathbf{x}_k^p, \mathbf{x}_k^v) \\ \mathbf{x}_k^p \\ \mathbf{x}_k^v \end{pmatrix} + \boldsymbol{\nu}_k, \quad (13)$$

where  $\boldsymbol{\nu}_k$  is a Gaussian measurement noise vector,  $\mathbf{z}_{p,k}$ ,  $\mathbf{z}_{v,k}$  and  $\mathbf{z}_{w,k}$  are the measured end-effector position, velocity and force acting on the end-effector, and where  $\mathbf{h}_w(\mathbf{x}_k^s, \mathbf{x}_k^p, \mathbf{x}_k^v)$  contains the expressions (3)-(5) in which  $\delta$  and  $v_t^p$  have been replaced with equations (6) and (7) and  $\kappa_k$  and  $\mu_k$  have been replaced by inverting the expressions (11). Thanks to the reparameterisation, the measurement equation indirectly *excludes negative values* of the stiffness and the coefficient of friction, such that an estimation algorithm using this parameter set cannot converge to non-physical values.

By combining equations (8)-(9) and (13), a compound state space model is obtained with a linear process equation  $\mathbf{x}_k = \mathbf{F}\mathbf{x}_{k-1} + \boldsymbol{\epsilon}_{k-1}$  and nonlinear measurement equation  $\mathbf{z}_k = \mathbf{h}(\mathbf{x}_k) + \boldsymbol{\nu}_k$ , where  $\mathbf{x}_k = (\mathbf{x}_k^p, \mathbf{x}_k^v, \mathbf{x}_k^a, \mathbf{x}_k^s)^T$  and  $\mathbf{z}_k = (\mathbf{z}_{w,k}, \mathbf{z}_{p,k}, \mathbf{z}_{v,k})^T$ .

### C. On-line hybrid estimation algorithm

For on-line estimation, techniques such as Kalman filters [12]–[14], particle filters [15] or moving horizon estimation [16] can be applied to the nonlinear state space model (8)-(9),(13). This paper adopts a Kalman filter approach which is computationally more attractive.

Unfortunately, the state space model contains an important *discontinuity* introduced by the signum function in the friction model, thus causing a significant amount of bimodality, such that a basic nonlinear Kalman filter cannot be applied *successfully*. This discontinuity can be dealt with, by considering the state space model to be that of a hybrid system with autonomous mode transitions [17], [18], where  $\text{sgn}(v_t^p)$  is a discrete state that depends on the continuous states. A velocity reversal can be regarded as an autonomous mode transition, where the sign of  $v_t^p$  is the guard condition. A number of ways exist to deal with hybrid systems with autonomous mode transitions, including particle filtering [15], Rao-Blackwellized particle filtering [18], hybrid mode estimation [17] and multiple model estimation [12]. In this paper, a multiple model approach is considered, since this is a computationally more attractive approach.

In the multiple model approach, the nonlinear hybrid state space model is split up into *two different models*. In the measurement equation  $\mathbf{h}(\mathbf{x}_k)$ ,  $\text{sgn}(v_t^p)$  is simply replaced by 1, yielding a first model with measurement equation  $\mathbf{h}^{(1)}(\mathbf{x}_k)$ , while for the second model, the measurement equation is  $\mathbf{h}^{(2)}(\mathbf{x}_k)$ , which is equal to  $\mathbf{h}(\mathbf{x}_k)$  except that  $\text{sgn}(v_t^p)$  has been replaced by  $-1$ . The process equation is the same for both models. For the estimation, two Kalman filters are run in parallel and their estimates and covariances are merged at every time-step using the first-order generalized pseudo-Bayesian (GPB1) algorithm [12]. Assuming a Gaussian probability with mean  $\hat{\mathbf{x}}_{k-1|k-1}$  and covariance  $\mathbf{P}_{k-1|k-1}$  at time-step  $k-1$ , the mean and covariance of the predicted probability density function (PDF) can be calculated as [12]

$$\hat{\mathbf{x}}_{k|k-1} = \mathbf{F}\hat{\mathbf{x}}_{k-1|k-1} \quad (14)$$

$$\mathbf{P}_{k|k-1} = \mathbf{F}\mathbf{P}_{k-1|k-1}\mathbf{F}^T + \mathbf{Q}_{k-1}. \quad (15)$$

Similarly, assuming a Gaussian probability with mean  $\hat{\mathbf{x}}_{k|k-1}$  and covariance  $\mathbf{P}_{k|k-1}$ , the measurement update for both models can be calculated as [12]

$$\hat{\mathbf{z}}_{k|k-1}^{(i)} = E[(\mathbf{h}^{(i)}(\mathbf{x}_k) + \boldsymbol{\nu}_k) | \mathbf{Z}_{k-1}], \quad (16)$$

$$\begin{aligned} \mathbf{P}_{zz,k|k-1}^{(i)} &= E[(\mathbf{h}^{(i)}(\mathbf{x}_k) + \boldsymbol{\nu}_k - \hat{\mathbf{z}}_{k|k-1}^{(i)}) \\ &\quad \times (\mathbf{h}^{(i)}(\mathbf{x}_k) + \boldsymbol{\nu}_k - \hat{\mathbf{z}}_{k|k-1}^{(i)})^T | \mathbf{Z}_{k-1}], \end{aligned} \quad (17)$$

$$\begin{aligned} \mathbf{P}_{zx,k|k-1}^{(i)} &= E[(\mathbf{h}^{(i)}(\mathbf{x}_k) + \boldsymbol{\nu}_k - \hat{\mathbf{z}}_{k|k-1}^{(i)}) \\ &\quad \times (\mathbf{x}_k - \hat{\mathbf{x}}_{k|k-1})^T | \mathbf{Z}_{k-1}], \end{aligned} \quad (18)$$

$$\mathbf{K}_k^{(i)} = (\mathbf{P}_{zx,k|k-1}^{(i)})^T (\mathbf{P}_{zz,k|k-1}^{(i)})^{-1}, \quad (19)$$

$$\mathbf{P}_{k|k}^{(i)} = \mathbf{P}_{k|k-1} - \mathbf{K}_k^{(i)} \mathbf{P}_{zz,k|k-1}^{(i)} (\mathbf{K}_k^{(i)})^T, \quad (20)$$

$$\hat{\mathbf{x}}_{k|k}^{(i)} = \hat{\mathbf{x}}_{k|k-1} + (\mathbf{K}_k^{(i)})(\mathbf{z}_k - \hat{\mathbf{z}}_{k|k-1}^{(i)}), \quad (21)$$

for  $i = 1, 2$ . To evaluate the expectations (16)-(21), different approaches exist, yielding different Kalman filter variants.

This paper uses an exact monomial integration rule of degree seven [19], yielding a higher-order variant of the unscented Kalman filter. After the measurement update, the estimates are merged as [12]

$$\hat{\mathbf{x}}_{k|k} = \sum_{i=1}^2 \hat{\mathbf{x}}_{k|k}^{(i)} \nu_k^{(i)} \quad (22)$$

$$\mathbf{P}_{k|k} = \sum_{i=1}^2 (\mathbf{P}_{k|k}^{(i)} + (\hat{\mathbf{x}}_{k|k} - \hat{\mathbf{x}}_{k|k}^{(i)})(\hat{\mathbf{x}}_{k|k} - \hat{\mathbf{x}}_{k|k}^{(i)})^T) \nu_k^{(i)}, \quad (23)$$

$$\text{where } \nu_k^{(i)} = \frac{\nu_{k|k-1}^{(i)} \mathbf{L}_k^{(i)}}{\sum_{j=1}^2 \nu_{k|k-1}^{(j)} \mathbf{L}_k^{(j)}}. \quad (24)$$

$\mathbf{L}_k^{(i)}$  is the likelihood calculated in the measurement update of model  $i$ .  $\mathbf{L}_k^{(i)}$  is defined for an  $n$ -dimensional state as

$$\mathbf{L}_k^{(i)} = \frac{\exp\left(-\frac{1}{2}(\mathbf{z}_k - \hat{\mathbf{z}}_{k|k-1}^{(i)})^T (\mathbf{P}_{zz,k|k-1}^{(i)})^{-1} (\mathbf{z}_k - \hat{\mathbf{z}}_{k|k-1}^{(i)})\right)}{|(2\pi)^n \mathbf{P}_{zz,k|k-1}^{(i)}|^{1/2}}$$

and  $\nu_{k|k-1}^{(1)} = P(\text{sgn}(v_{t,k}^p) = 1 | \mathbf{Z}_{k-1})$  is the *predicted probability* that  $\text{sgn}(v_t^p)$  will be 1 at time-step  $k$  and  $\nu_{k|k-1}^{(2)} = P(\text{sgn}(v_{t,k}^p) = -1 | \mathbf{Z}_{k-1}) = 1 - \nu_{k|k-1}^{(1)}$ .

$\nu_{k|k-1}^{(1)}$  can be calculated by drawing samples  $\hat{\mathbf{x}}_{k|k-1}^{(j)}$  from the multivariate Gaussian distribution with mean  $\hat{\mathbf{x}}_{k|k-1}$  and covariance  $\mathbf{P}_{k|k-1}$  and calculating the proportion of samples for which  $v_t^p(\hat{\mathbf{x}}_{k|k-1}^{(j)}) > 1$ .

#### D. Event-triggered estimation

Instead of running the estimation algorithm in a time-triggered fashion, an event-triggered approach is adopted, which is motivated by three important considerations. First, the estimation algorithm chosen in Section III-C is only approximate, because Kalman filters for *nonlinear systems* are always approximate, and the multiple model approach adopted in Section III-C is also only approximate. Because of the approximate nature of the algorithm, it is only useful to process measurements when they are informative, while processing uninformative measurements does not yield any new information and can even result in *information loss*. Measurements can only contain *significant new* information if the robot has moved while remaining in contact, either normal or tangential to the environment surface or a combination of both.

Second, as mentioned in Section III-A, the geometric and dynamic parameters do not vary with time, but instead with the *position* of the probe end-point on the environment surface. Hence, it is reasonable to increase the uncertainty on the parameters at time  $T + \Delta t$  only when the probe end-point has moved by a certain threshold amount  $\Delta s_{t,m}$  since time  $T$ . In other words if  $\Delta s_t^p = \int_T^{T+\Delta t} v_t^p(t) dt > \Delta s_{t,m}$ .

Third, the chosen friction model is not able to account for the frictional behavior in the sticking phase. Neither the evolution of the coefficient of friction, nor the behavior as a function of the tangential velocity is correctly modelled by process model (9) and model (2). Therefore, it is only

---

#### Algorithm 1 The event-triggered estimation algorithm.

---

**if**  $\Delta s_t^p > \Delta s_{t,m}$  **then**

**Process update:** Increase uncertainty on states and parameters and calculate  $\hat{\mathbf{x}}_{k|k-1}$ ,  $\mathbf{P}_{k|k-1}$   
Reset  $\Delta s_t^p$

**else**

**Reduced process update:** Increase uncertainty only on states and calculate  $\hat{\mathbf{x}}_{k|k-1}$ ,  $\mathbf{P}_{k|k-1}$   
 $\Delta s_t^p = \Delta s_t^p + \hat{v}_t^p T_s$

**end if**

Sample  $\hat{\mathbf{x}}_{k|k-1}^{(j)}$  and calculate  $v_t^p(\hat{\mathbf{x}}_{k|k-1}^{(j)})$

Calculate  $\nu_{k|k-1}^{(1)}$ ,  $\nu_{k|k-1}^{(2)}$  and  $\hat{v}_t^p$

**if**  $\hat{v}_t^p > v_{t,m}$  **then**

**Measurement update 1:** Calculate  $\hat{\mathbf{x}}_{k-1|k-1}^{(1)}$ ,  $\mathbf{P}_{k-1|k-1}^{(1)}$

**Measurement update 2:** Calculate  $\hat{\mathbf{x}}_{k-1|k-1}^{(2)}$ ,  $\mathbf{P}_{k-1|k-1}^{(2)}$

**Merge estimates:** Calculate  $\hat{\mathbf{x}}_{k-1|k-1}$ ,  $\mathbf{P}_{k-1|k-1}$

**else**

**Reduced measurement update:** Calculate  $\hat{\mathbf{x}}_{k-1|k-1}$ ,  $\mathbf{P}_{k-1|k-1}$  using only  $\mathbf{z}_{p,k}$ ,  $\mathbf{z}_{v,k}$

**end if**

---

reasonable to process force measurements when the tangential velocity of the probe end-point along the environment surface is sufficiently high. In other words, if  $v_t^p > v_{t,m}$ .

The above considerations give rise to Algorithm 1, which is executed at a fixed frequency, but where the process and measurement updates are executed in an event-triggered way. Due to the choice of the sampling approach to calculate  $\nu_{k|k-1}^{(i)}$ , a set of samples  $v_t^p(\hat{\mathbf{x}}_{k|k-1}^{(j)})$ , is available, from which a nominal estimate  $\hat{v}_t^p$  can be obtained as the mean.  $\Delta s_t^p$  is calculated by integrating  $\hat{v}_t^p$ . Increasing the uncertainty on the parameters in an event-triggered way is beneficial for convergence and reduces the need for *persistent excitation*, while processing the force measurements only in the sliding phase *increases the robustness* because the estimation algorithm is not confronted with measurements that *cannot be explained* by the measurement equations.

## IV. EXCITATION

This section discusses some heuristic considerations regarding excitation signals. Determining sufficiently exciting signals by solving an optimization problem, is known as active sensing [20]. In [20], it is found that excitation signals for geometric parameter estimation, determined by active sensing, do not seem to differ greatly from heuristically conceived signals. Therefore, this paper limits itself to an intuitive choice of excitation signals.

A number of considerations to improve the observability of the geometric and dynamic parameters are given below:

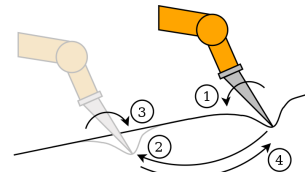


Fig. 2. The excitation used to explore an unknown environment.

- the probe vertex coordinates  $x^p, y^p$ : the moment acting on the end-effector reveals information about the coordinates of the probe vertex (equation (5)). By varying the moment by rotating around the probe vertex, these parameters can be estimated more accurately.
- the environment orientation  $\phi$  and the coefficient of friction  $\mu$ : the forces acting on the end-effector provide information about the orientation of the environment, but this information is disturbed by friction forces. By changing the sign of the tangential velocity of the probe vertex, the force direction will vary almost discontinuously, thus allowing to discern the friction component. Velocity reversals significantly improve the estimation accuracy of both the environment orientation and the coefficient of friction. In fact, the friction coefficient and the environment orientation are difficult to observe simultaneously if no velocity reversals occur, as a change in the direction of the measured force may be attributed to a change in the orientation of the environment, or a change in the coefficient of friction.
- the environment position  $d$ : the estimation accuracy of  $d$  is affected by the estimation accuracy of  $x^p, y^p$  and  $\phi$ , such that excitation signals which increase the observability of  $x^p, y^p$  and  $\phi$  will also indirectly improve the observability of  $d$ .
- the environment stiffness  $\kappa$ : the stiffness can be estimated accurately by varying the environment deformation. Hence, increasing and decreasing the deformation of the environment improves the stiffness estimation.

Based on these considerations, excitation signals as shown schematically in Fig. 2 are applied. The motion corresponds largely to what humans usually do when exploring an unknown surface with a probe, namely sliding back and forth, while orienting the probe in the opposite direction of the sliding direction. During the sliding motions, the environment is deformed in a sinusoidal way.

## V. EXPERIMENTAL RESULTS

The approach explained in Section III is validated experimentally on the setup shown in Fig. 3. The absolute accuracy of the end-effector position calculated from the encoder measurements is not satisfactory due to errors in the forward kinematics. Therefore, a tool with markers is mounted on the robot end-effector, such that the end-effector position can be measured directly, using a Metris K600 camera system. The

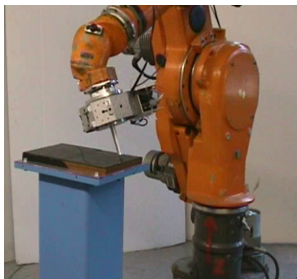


Fig. 3. A robot using a probe to explore an unknown environment.

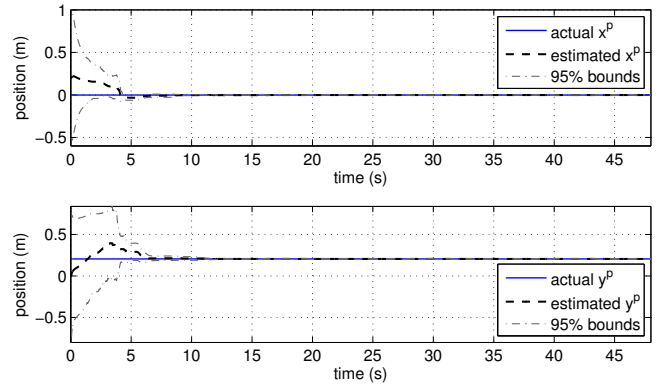


Fig. 4. Estimated x- and y-coordinate  $\hat{x}^p$  and  $\hat{y}^p$  of the probe vertex.

probe is mounted on the tool and is brought into contact with the environment, which consists of a thick layer of rubber. A position trajectory, that satisfies the heuristic requirements discussed in Section IV, is applied to the robot to excite the environment. The applied trajectory is calculated beforehand based on a first rough estimate of the values of the geometric and the dynamic parameters, such that contact between the robot and the environment is maintained and in such a way that interaction forces do not exceed 50 N.

The estimation starts when contact is made and measurements are processed at 25Hz. In Fig. 4, the estimated coordinates  $\hat{x}^p$  and  $\hat{y}^p$  of the probe end-point are shown. In Fig. 5, the estimated environment orientation  $\hat{\phi}$  and offset  $\hat{d}$  are shown. In Fig. 6, the estimated stiffness  $\hat{\kappa}$  and coefficient of friction  $\hat{\mu}$  are shown, which are calculated using numerical integration as the expected values of  $(\exp(\tilde{\kappa}_k)\bar{\kappa} + 0)/(\exp(\tilde{\kappa}_k) + 1)$  and  $(\exp(\tilde{\mu}_k)\bar{\mu} + 0)/(\exp(\tilde{\mu}_k) + 1)$  respectively. In Fig. 7, the estimated tangential velocity  $\hat{v}_t^p$  of the probe end-point is shown. Initially, the tangential velocity is not accurately estimated. As the accuracy of the geometric parameters increases, however, the tangential velocity is estimated more accurately and the estimates of the environment stiffness and friction coefficient converge to the reference values. The convergence of the parameters is strongly linked to the excitation. The accuracy of the geometric parameters improves considerably, when the probe

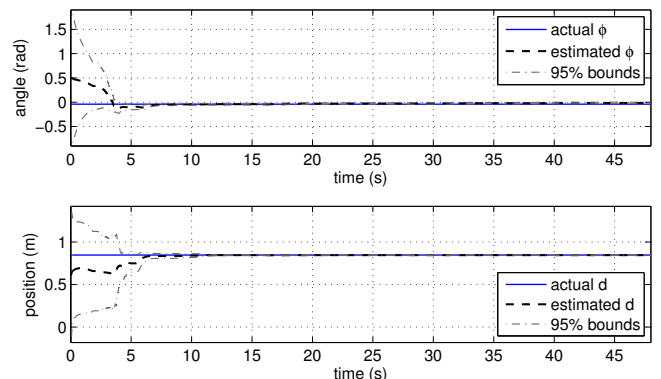


Fig. 5. Estimated environment surface orientation  $\hat{\phi}$  and offset  $\hat{d}$ .

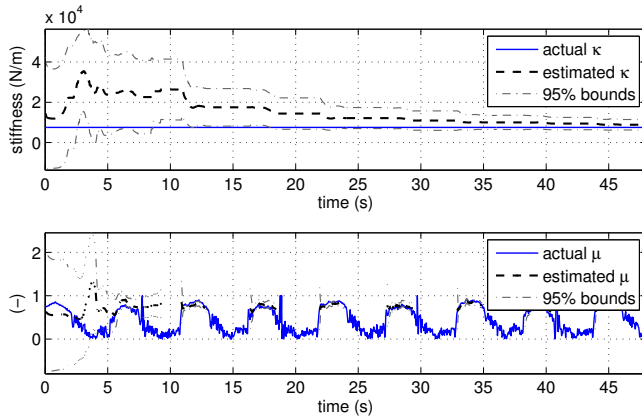


Fig. 6. Estimated environment stiffness  $\hat{\kappa}$  and coefficient of friction  $\hat{\mu}$ .

is rotated for the first time at  $t = 2.5$  s, while the stiffness estimates  $\hat{\kappa}$  are only updated significantly when the environment is deformed during the sliding phase. The reference values for the geometric parameters were measured while the values for the dynamic parameters were calculated off-line from the gathered measurements using the reference values for the geometric parameters. The parameter estimates are not updated when the tangential velocity is low. Therefore, the estimated coefficient of friction is not shown at these instances. The accuracy of the parameters estimated by the algorithm is of the same order of magnitude as the confidence in the reference values, namely  $2 \cdot 10^{-3}$  m and  $3 \cdot 10^{-2}$  rad for the geometric parameters and  $500 \frac{N}{m}$  and  $3 \cdot 10^{-3}$  for the stiffness and the coefficient of friction respectively. Since the end-effector position and velocity are measured directly, the estimation accuracy is naturally quite good. Therefore, the figures of the estimated end-effector position, velocity and acceleration are omitted.

## VI. CONCLUSIONS AND FUTURE WORK

In this paper, a Kalman filter based identification algorithm is proposed to simultaneously estimate contact dynamics parameters and geometric uncertainties on-line, which is able to deal with the discontinuity introduced by the friction model. In addition, physical constraints on the dynamic parameters are enforced by a reparameterisation, and convergence and robustness are improved by running the algorithm in an event-triggered fashion. Experimental results are presented, which illustrate the viability of the approach.

Future work consists of integrating the identification algorithm with a control algorithm and path planning algorithm

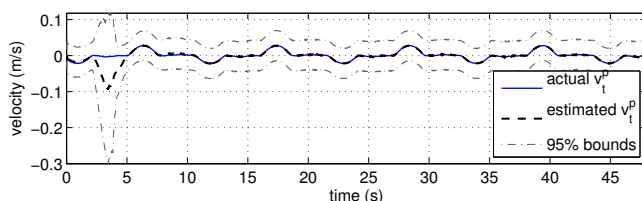


Fig. 7. Estimated tangential velocity  $\hat{v}_t^p$  of the probe vertex.

to allow fully autonomous environment exploration, and extension of the proposed approach to 3D cases, with single or multiple contact points.

## VII. ACKNOWLEDGEMENTS

The authors gratefully acknowledge the financial support by K.U.Leuven's Concerted Research Action GOA/05/10, the Prof. R. Snoeys Foundation and K.U.Leuven's CoE EF/05/006 Optimization in Engineering Center (OPTEC).

## REFERENCES

- [1] S.-T. Lin and H. K. Yae, "Identification of unknown payload and environmental parameters for robot compliant motion," in *Proceedings of the American Control Conference*, Chicago, 1992, pp. 2952–2956.
- [2] S. K. Singh and D. O. Popa, "An analysis of some fundamental problems in adaptive control of force and impedance behavior: Theory and experiments," *IEEE Transactions on Robotics and Automation*, vol. 11, no. 1, pp. 912–921, 1995.
- [3] L. Love and W. Book, "Environment estimation for enhanced impedance control," in *Proceedings of the IEEE International Conference on Robotics and Automation*, Nagoya, Japan, 1995.
- [4] H. Seraji and R. Colbaugh, "Force tracking in impedance control," *The International Journal of Robotics Research*, vol. 16, no. 1, pp. 97–117, 1997.
- [5] S. Blouin, R. Hurteau, and R. Gourdeau, "Identification paramétrique d'un environnement par une tâche de contact d'un manipulateur robotique," in *Proceedings of the International Conference on Industrial Automation*, 1999, pp. 921–924.
- [6] R. Kikuuwe and T. Yoshikawa, "Robot perception of environment impedance," in *Proceedings of the IEEE International Conference on Robotics and Automation*, Washington DC, VA, 2002, pp. 1661–1666.
- [7] —, "Recognizing surface properties using impedance perception," in *Proceedings of the IEEE International Conference on Robotics and Automation*, Taipei, Taiwan, 2003, pp. 1539–1544.
- [8] N. Diolaiti, C. Melchiorri, and S. Stramigioli, "Contact impedance estimation for robotic systems," *IEEE Transactions on Robotics*, vol. 21, no. 5, pp. 925–935, 2005.
- [9] D. Erickson, M. Weber, and I. Sharf, "Contact stiffness and damping estimation for robotic systems," *The International Journal of Robotics Research*, vol. 22, no. 1, pp. 41–57, 2003.
- [10] R. Smits, H. Bruyninckx, W. Meeussen, J. Baeten, P. Slaets, and J. De Schutter, "Model based position-force-vision sensor fusion for robot compliant motion control," in *IEEE International Conference on Multisensor Fusion and Integration for Intelligent Systems*, Heidelberg, Germany, 2006, pp. 501–506.
- [11] N. L. Johnson, "Systems of frequency curves generated by methods of translation," *Biometrika*, vol. 36, no. 1, pp. 149–176, 1949.
- [12] Y. Bar-Shalom and X. Li, *Estimation and Tracking, Principles, Techniques, and Software*. Artech House, 1993.
- [13] S. J. Julier and J. K. Uhlmann, "A new extension of the Kalman filter to nonlinear systems," in *International Symposium on Aerospace/Defense Sensing, Simulation and Controls*. Orlando, FL: SPIE, 1997.
- [14] T. Lefebvre, H. Bruyninckx, and J. De Schutter, "Kalman Filters for nonlinear systems: a comparison of performance," *International Journal of Control*, vol. 77, no. 7, pp. 639–653, 2004.
- [15] A. Doucet, S. Godsill, and C. Andrieu, "On sequential monte carlo sampling methods for Bayesian filtering," *Statistics and Computing*, vol. 10, pp. 197–208, 2000.
- [16] C. V. Rao, "Moving horizon strategies for the constrained monitoring and control of nonlinear discrete-time systems," Ph.D. dissertation, University of Wisconsin Madison, 2000.
- [17] B. C. Williams, M. Hofbaur, and T. Jones, "Mode estimation of probabilistic hybrid systems," in *Proceedings of the International Joint Conference on Artificial Intelligence*, 2001.
- [18] S. Funiak, "State estimation of probabilistic hybrid systems," Ph.D. dissertation, Massachusetts Institute of Technology, 2004.
- [19] U. Lerner, "Hybrid Bayesian networks for reasoning about complex systems," Ph.D. dissertation, Stanford University, Department of Computer Science, 2002.
- [20] T. Lefebvre, "Contact modelling, parameter identification and task planning for autonomous compliant motion using elementary contacts," Ph.D. dissertation, Katholieke Universiteit Leuven, Department of Mechanical Engineering, Belgium, 2003.